AGU PUBLICATIONS

Geophysical Research Letters

RESEARCH LETTER
10.1002/2014GL060274

Key Points:
- 2014 Iquique earthquake rupture process inverted applying a novel formulation
- Stress release of foreshocks may explain the initial rupture phase of main shock
- Foreshock activity and slow slip contributed to the triggering of the main shock

Supporting Information:
- Readme
- Figures S1 and S2

Correspondence to:
Y. Yagi,
yagi-y@geol.tsukuba.ac.jp

Citation:
Yagi, Y., R. Okuwaki, B. Enescu, S. Hirano, Y. Yamagami, S. Endo, and T. Komoro (2014), Rupture process of the 2014 Iquique Chile Earthquake in relation with the foreshock activity, *Geophys. Res. Lett.*, *41*, 4201–4206, doi:10.1002/2014GL060274.

Received 18 APR 2014
Accepted 2 JUN 2014
Accepted article online 5 JUN 2014
Published online 27 JUN 2014

Rupture process of the 2014 Iquique Chile Earthquake in relation with the foreshock activity

Yuji Yagi[1], Ryo Okuwaki[2], Bogdan Enescu[1], Shiro Hirano[3], Yuta Yamagami[2], Suguru Endo[2], and Takuya Komoro[2]

[1]Faculty of Life and Environmental Sciences, University of Tsukuba, Tsukuba, Japan, [2]Graduate School of Life and Environmental Sciences, University of Tsukuba, Tsukuba, Japan, [3]Faculty of Engineering, Information and Systems, University of Tsukuba, Tsukuba, Japan

Abstract The rupture process of the 2014 Iquique, Chile earthquake is inverted from teleseismic *P* wave data applying a novel formulation that takes into account the uncertainty of Green's function, which has been a major error source in waveform inversion. The estimated seismic moment is 1.5×10^{21} Nm (*Mw* = 8.1), associated with a 140 km long and 140 km wide fault rupture along the plate interface. The source process is characterized by unilateral rupture propagation. During the first 20 s, the dynamic rupture front propagated from the hypocenter to the large asperity located about 50 km southward, crossing a remarkably active foreshock area at high velocity (of about 3.0 km/s), but small and irregular seismic moment release rate. Our result may suggest that the 20 s long initial phase was influenced by the stress drop due to the foreshock activity near the main shock hypocenter. Moreover, the 2 week long swarm-like foreshock activity migrating roughly at 5 km/day toward the main shock hypocenter, and possibly associated slow slip, contributed to the stress accumulation prior to the *Mw* 8.1 megaquake. The main shock initial rupture phase might have triggered the rupture of the large asperity, which had large fracture energy.

1. Introduction

On the night of 1 April 2014, a great thrust earthquake (*Mw* 8.1) occurred off Iquique, northern Chile. The earthquake information determined by the Centro Sismológico Nacional (CSN), the University of Chile [http://www.sismologia.cl; last access on 18 April 2014] is as follows: origin time = 1/4/2014 23:46:45 (UT); epicenter = 19.572S, 70.908 W; depth = 38.9 km; *Mw* = 8.2. In the off Iquique region, the Nazca Plate is subducting at a rate of about 63 mm/y beneath the South American Plate along the Peru-Chile trench [*Kendrick et al.*, 2003], where several great interplate earthquakes have been observed since the dawn of history. The coupling rate on the plate interface has been estimated from the Global Positioning System (GPS) data [e.g., *Chlieh et al.*, 2011; *Moreno et al.*, 2011]. Figure 1 shows the aftershock activity during the first 2 days after the megaquake (hypocenters determined by CSN) and the focal mechanism of the main shock determined in the present study. The main shock mechanism is consistent with the tectonic stress buildup at the plate boundary. It is particularly notable that this megathrust event occurred within a plate boundary segment that has not been ruptured since the great 1877 event, with an estimated magnitude of about 8.8 [*Chlieh et al.*, 2011; Figure 1].

In this study we estimate the detailed rupture process of the 2014 off Iquique earthquake from teleseismic *P* wave data, using a newly developed inversion method [*Yagi and Fukahata*, 2011a] that takes into account the uncertainty of Green's function, which has been a major error source in waveform inversion. Based on the rupture process of the main shock and characteristic foreshock activity, we propose a scenario to explain the foreshock-main shock interaction.

2. Inversion Analysis

To image the rupture process of the off Iquique earthquake, we inverted teleseismic *P* wave data recorded at 48 broadband network stations, which were selected to ensure adequate azimuthal coverage and data quality. The observed waveforms were shifted on the basis of their first arrival time and then converted into velocity waveforms with a sampling interval of 0.8 s. For mitigating the effect of aliasing and low-frequency noise, we applied a Butterworth band-pass filter between 0.001 and 0.36 Hz before re-sampling.

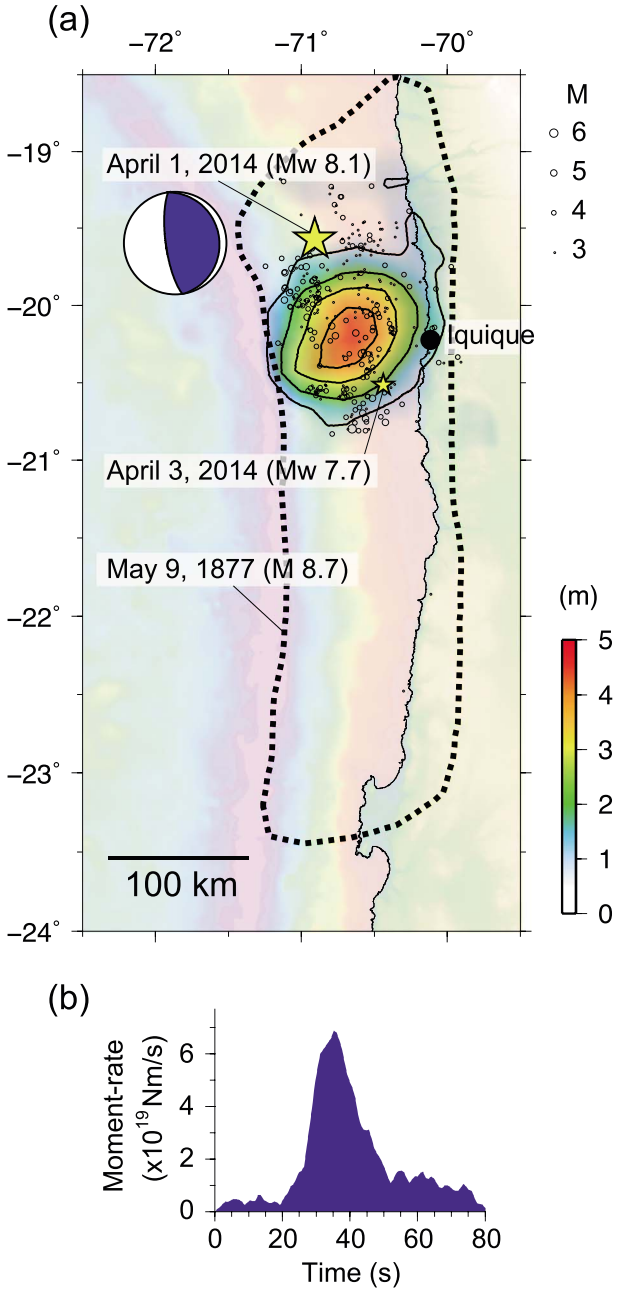

Figure 1. Total slip distribution, aftershock distribution, and moment-rate function. (a) Map view of inverted total slip distribution of the 2014 off Iquique earthquake. Large and small stars indicate the epicenter of the main shock and the largest aftershock, respectively. Also shown are the focal mechanism of main shock determined in this study and the first 2 days aftershocks (black circles), determined by the Centro Sismológico Nacional (CSN), the University of Chile. The seismic source area of 1877 off Iquique (*M* 8.8) earthquake [*Chlieh et al.*, 2011] is indicated by a thick dotted line. Topography and bathymetry are from ETOPO1 [*Amante and Eakins*, 2009]. (b) The moment-rate function of the main shock.

Waveform inversion is widely used for constructing seismic source models; however, models may differ substantially for the same earthquake [e.g., *Beresnev*, 2003; *Razafindrakoto and Mai*, 2014]. Waveform inversion is especially problematic for large earthquakes with a long source time function, because seismic data for such events are contaminated by various later phases, which are difficult to calculate accurately because of the limited accuracy of the Green's function. To cope with this problem, we applied the newly developed inversion method of *Yagi and Fukahata* [2011a], in which the uncertainty of the Green's function is taken into account. One of the clear advantages of this method is that the effect of correlated modeling errors is naturally mitigated, therefore making possible to discuss the detailed rupture process, including the small initial rupture phase [*Yagi and Fukahata*, 2011b]. According to this method, the smoothness of slip distribution is objectively determined from the observed data, based on Akaike's Bayesian Information Criterion (ABIC) [*Akaike*, 1980; *Yabuki and Matsu'ura*, 1992] and the non-negative constraint for slip is not needed.

We calculated the theoretical Green's function using the method of *Kikuchi and Kanamori* [1991] with a sampling rate of 0.1 s. To explain the teleseismic waveforms, we slightly modified the structure model of *Delouis et al.* [2009]. We assumed that the faulting occurred on a single plane and adopted a hypocenter (19.572S, 70.908 W; depth = 22 km) and fault mechanism (strike 350°, dip 15°) that were slightly modified from the CSN hypocenter and the Global Centroid-Moment-Tensor (GCMT) solution [http://www.globalcmt.org; last access on 18 April 2014], respectively. The fault area used for the source process inversion was taken as 225 km × 195 km, which was expanded into bilinear B-splines with an interval of 15 km. Recent studies show that great earthquakes have a complex rupture manner including back propagating rupture and slip reactivation around the hypocenter [e.g., *Ide et al.*, 2011]. Therefore, we took a slip-rate duration of 56 s on each fault patch, which was expanded into linear B-splines with an interval of 0.8 s. Based on preliminary analyses, we assumed that the rupture front velocity can be up to 3.4 km/s, which yielded the start time of the linear B-splines at each sub-fault. We also assumed no slip after 80 s from the initial rupture.

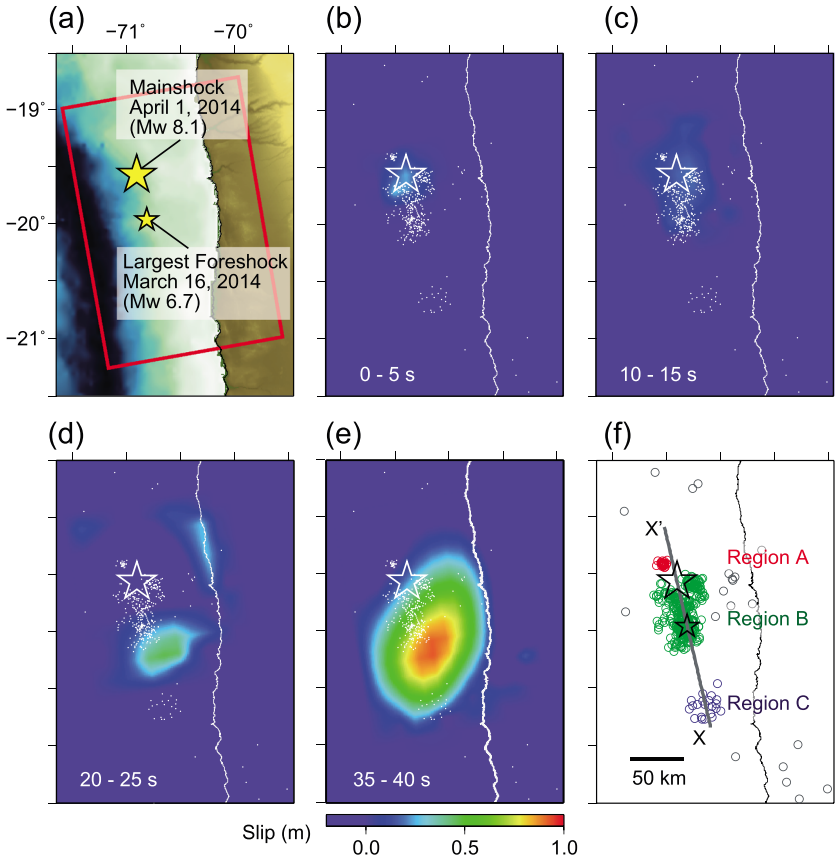

Figure 2. Snapshots of the main shock , projected along the average slip vector direction, at specific time steps and seismicity before the main shock. (a) The rectangle indicates the fault plane. Large and small yellow stars indicate the epicenter of the main shock and largest foreshock, respectively. (b), (c), (d), and (e) Snapshots of slip distribution from 0 to 5 s, 10 to 15 s, 20 to 25 s, and 35 to 40 s, respectively, after earthquake initiation. White dots show epicenters of earthquakes ($M \geq 3.0$) occurred from 1 January 2014 to the origin time of the main shock determined by CSN. (f) Foreshocks in region A (red circles), region B (green circles), and region C (blue circles). The solid line X-X' indicates the projection direction used in Figure 3.

3. Results

The inverted slip distribution and moment rate function of the main shock are shown in Figure 1 (see supporting information Figs. S1 and S2 for the waveform fitting results and projection of the slip distribution on the main shock fault, respectively). The maximum slip was about 4.6 m to the south of the *Mw* 8.1 epicenter. The obtained total seismic moment was 1.5×10^{21} Nm ($Mw = 8.1$), which agrees with the GCMT solution: 1.6×10^{21} Nm. The effective rupture area was roughly estimated to be 140 km long and 140 km wide along the plate interface. The earthquake started abruptly but continued afterward with low-rate seismic moment release during the first 20 s. The seismic moment during the first 20 s is 7.6×10^{19} Nm, only 5% of the total seismic moment. After the initial stage, the moment rate rapidly increased and reached 6.8×10^{19} Nm/s at 35 s from the initial break and then rapidly decreased with time.

Figure 2 shows snapshots of slip distribution at specific time steps together with the seismicity ($M \geq 3.0$) from 1 January 2014 to the origin time of the main shock (hypocenters determined by CSN). We can detect three high-seismicity areas (Figure 2f) on the source region of the main shock (Figures 2b–2e). In the northern region (region A, in Figure 2f), the seismicity became active from the beginning of February to the middle of March. In the middle region B, the largest foreshock (*M*6.7) occurred on 16 March 2014, and many aftershocks of this largest foreshock were observed afterward. In the southern region C, the seismicity became active during January 2014.

The rupture started in a low-seismicity area in-between the high-seismicity regions A and B, and then propagated southward from hypocenter at a low slip-rate. The main rupture started at 20 s after the initial

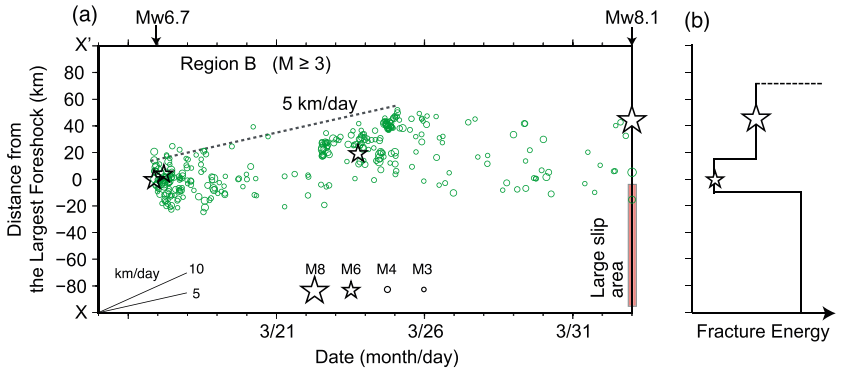

Figure 3. Space-time plots of seismicity in region B (Figure 2f) and schematic diagram showing the fracture energy distribution. (a) Green open circles denote events occurred in region B ($M \geq 3.0$) plotted as function of time and distance from the *Mw* 6.7 foreshock epicenter, along the X-X′ line (Figure 2f). Black dashed line represents the approximate location of the earthquake migration front. (b) Qualitative fracture energy distribution along the X-X′ line. Large and small stars represent epicenters of main shock and the *Mw* 6.7 foreshock, respectively.

break in the southern edge of region B. After that, the slip-rate in the main asperity area, centered about 80 km south from the epicenter, accelerated until 55 s. Note that the location of the main asperity of the main shock corresponds well to a gap between two highly active seismic patches (regions B and C). As shown in Figure 1a, the largest aftershock (*Mw* 7.7) occurred at the southern edge of the large co-seismic slip area of the main shock. The main shock waveform pulses are relatively narrow at azimuths similar to those of the rupture propagation direction and become broader at stations located at opposite azimuths.

4. Discussion

During the first 20 s, the dynamic rupture front of the main shock propagated from the hypocenter to the large asperity area via the foreshock region B at a high velocity of about 3.0 km/s, while the moment rate released during this initial phase was small and irregular. Assuming that the stress drop of foreshocks is not unusually small, we hypothesize that it might have contributed to such initial phase features by reducing the potential of a large rupture in region B. Note that similar irregular initial phases have been reported for various other earthquakes [e.g., *Beroza and Ellsworth*, 1996; *Ellsworth and Beroza*, 1998], and our result is consistent with the underlying mechanisms discussed in such studies [e.g., *Ellsworth and Beroza*, 1995].

A remarkable and extensively analyzed foreshock sequence was observed before the 2011 Tohoku-oki megathrust earthquake [e.g., *Ando and Imanishi*, 2011; *Kato et al*., 2012; *Marsan and Enescu*, 2012]. To compare the 2014 off Iquique foreshock sequence with the one preceding the 2011 Tohoku-oki earthquake, we concentrate our discussion on the foreshock activity in region B of this study. As shown in Figure 2f, the foreshock region B extends about 60 km long and 30 km wide along the plate interface. Figure 3a shows a space-time plot of seismicity in the source region of the Iquique main shock between 16 March 2014 and the origin time of the main shock. The foreshock activity migrates toward the rupture initiation point of the main shock at a speed of about 5 km/day, which is similar with the Tohoku-oki earthquake case: about 2–5 km/day [*Kato et al*., 2012]. In the case of the Tohoku-oki earthquake, a remarkable slow-slip event accompanying the characteristic foreshock activity was detected by acoustic GPS and pressure gauges [*Ohta et al*., 2012], repeating earthquakes [*Kato et al*., 2012], as well as the analysis of broadband F-net waveform data [*Marsan and Enescu*, 2012]. In general, large slow-slip events have been commonly observed after thrust earthquakes in subduction zones; these events are known as afterslip or post-seismic slip [e.g., *Heki et al*., 1997; *Chlieh et al*., 2007; *Suito et al*., 2011]. The slow-slip event is triggered in an area surrounding the seismic source region of a large earthquake and then contributes to the stress accumulation prior to a next large earthquake [e.g., *Yagi et al*., 2001]. Considering the resemblance between the two foreshock sequences (i.e., Tohoku-oki and off Iquique) and the peculiarity of thrust earthquakes in subduction zones, we hypothesize that in the case of the 2014 event as well slow slip—associated with the foreshock sequence—might have migrated toward the rupture initiation point of the main shock and contributed to the nucleation of this great earthquake. It is also reasonable to assume that static stress transfer [*Stein*, 1999] from nearby large foreshocks to the main shock

asperity region might have contributed to the triggering of the megathrust event; a similar mechanism was proposed for the case of the 2011 Tohoku-oki [e.g., *Marsan and Enescu*, 2012].

Although it is beyond the scope of this paper to build a detailed physical model, it is worth providing a hypothetic scenario underlying the complex rupture of this sequence. The hierarchical asperity model proposed by *Ide and Aochi* [2005], *Hori and Miyazaki* [2011], and *Noda et al*. [2013] may provide an appropriate framework. Figure 3b shows a schematic, qualitative diagram of the fracture energy distribution before the largest foreshock, as suggested by the observations and based on the delayed cascade-up model [*Noda et al*., 2013]. Thus, the area of the *M*6.7 foreshock (Figure 3b) and its aftershocks can be regarded as having the smallest fracture energy (thereby critical crack length) compared with the surrounding areas: otherwise, the rupture of the *M*6.7 event would not have stopped, but instead would have grown up into a larger event. Furthermore, the foreshock (and possibly associated slow slip) migration toward north suggests that this area (where the main shock initiated) had a "middle-sized" critical crack length. Finally, the main shock asperity area (to the south) was likely the "strongest" patch (highest fracture energy region); the rupture here was dynamically triggered by the propagation of the initial rupture phase of the main shock. The relation between the foreshock activity and main shock rupture process can thus provide an insight into the cascade-up rupture growth of great interplate earthquakes.

5. Conclusions

We have estimated the rupture process of the 2014 off Iquique earthquake and discussed its characteristics in relation to the preceding seismicity in the region. The megathrust event ruptured a 140 km long by 140 km wide fault along the plate interface and released a seismic moment of 1.5×10^{21} Nm ($Mw = 8.1$).

A remarkable foreshock sequence started about 2 weeks before the main shock and migrated northward, at a speed of about 5 km/day, to the hypocenter of the megathrust event. The rupture of the main shock propagated into an opposite direction (toward south) crossing the foreshock area at high velocity (of about 3.0 km/s), but with a small and irregular seismic moment release rate. The stress drop during previous foreshocks may explain such characteristics of the initial rupture phase.

The foreshock activity and possibly associated slow slip likely contributed to the triggering of the main shock. The initial rupture phase of the main shock might have triggered the rupture of the large asperity, which had large fracture energy.

Acknowledgments

Waveform data obtained by the Antarctic Seismographic Argentinean Italian Network (ASAIN), Alaska Tsunami Warning Seismic System, Caribbean Network, Incorporated Research Institutions for Seismology (IRIS), China Digital Seismic Network, GEOSCOPE, Global Telemetered Southern Hemisphere Network, IRIS/IDA Network, and IRIS/USGS Global Seismograph Network (GSN) were supplied by IRIS. We used hypocenters determined by CSN and moment tensor solutions determined by the Global CMT project. We also used the topography and bathymetry from ETOPO1. We thank W. L. Ellsworth, A. Tassara, T. Takagawa, L. Meng, and C. Ji for useful comments. We also acknowledge the comments by anonymous reviewers in improving the manuscript. This study was supported by Grant-in-Aid for Scientific Research 24540450, 24101012, and 24310133 of the Japan Ministry of Education, Culture, Sports, Science, and Technology to YY. This research was also supported by the Science and Technology Research Partnership for Sustainable Development (SATREPS), Japan Science and Technology Agency (JST)/Japan International Cooperation Agency (JICA). Some of the figures were made using the public domain Generic Mapping Tools [*Wessel and Smith*, 1998].

The Editor thanks two anonymous reviewers for their assistance in evaluating this paper.

References

Akaike, H. (1980), Likelihood and the Bayes procedure, in *Bayesian Statistics*, edited by J. M. Bernardo et al., pp. 143–166, Univ. Press, Valencia, Spain, doi:10.1007/BF02888350.

Amante, C., and B. W. Eakins (2009), ETOPO1 1 Arc-Minute Global Relief Model: Procedures, Data Sources and Analysis, *NOAA Technical Memorandum NESDIS NGDC-24*, 19.

Ando, R., and K. Imanishi (2011), Possibility of *Mw* 9.0 mainshock triggered by diffusional propagation of after-slip from *Mw* 7.3 foreshock, *Earth Planets Space*, *63*(7), 767–771, doi:10.5047/eps.2011.05.016.

Beresnev, I. A. (2003), Uncertainties in finite-fault slip inversions: To what extent to believe? (A critical review), *Bull. Seismol. Soc. Am.*, *93*(6), 2445–2458, doi:10.1785/0120020225.

Beroza, G. C., and W. L. Ellsworth (1996), Properties of the seismic nucleation phase, *Tectonophysics*, *261*, 209–227, doi:10.1016/0040-1951(96)00067-4.

Chlieh, M., et al. (2007), Coseismic slip and afterslip of the great *Mw* 9.15 Sumatra–Andaman earthquake of 2004, *Bull. Seismol. Soc. Am.*, *97*(1A), S152–S173, doi:10.1785/0120050631.

Chlieh, M., H. Perfettini, H. Tavera, J. P. Avouac, D. Remy, J. M. Nocquet, F. Rolandone, F. Bondoux, G. Gabalda, and S. Bonvalot (2011), Interseismic coupling and seismic potential along the Central Andes subduction zone, *J. Geophys. Res.*, *116*, B12405, doi:10.1029/2010JB008166.

Delouis, B., M. Pardo, D. Legrand, and T. Monfret (2009), The *Mw* 7.7 Tocopilla earthquake of 14 November 2007 at the southern edge of the northern Chile seismic gap: Rupture in the deep part of the coupled plate interface, *Bull. Seismol. Soc. Am.*, *99*(1), 87–94, doi:10.1785/0120080192.

Ellsworth, W. L., and G. C. Beroza (1995), Seismic evidence for an earthquake nucleation phase, *Science*, *268*(5212), 851–855, doi:10.1126/science.268.5212.851.

Ellsworth, W. L., and G. C. Beroza (1998), Observation of the seismic nucleation phase in the Ridgecrest, California, earthquake sequence, *Geophys. Res. Lett.*, *25*(3), 401–404, doi:10.1029/97GL53700.

Heki, K., S. Miyazaki, and H. Tsuji (1997), Silent fault slip following an interplate thrust earthquake at the Japan Trench, *Nature*, *386*, 595–598, doi:10.1038/386595a0.

Hori, T., and S. Miyazaki (2011), A possible mechanism of M 9 earthquake generation cycles in the area of repeating M 7-8 earthquakes surrounded by aseismic sliding, *Earth Planets Space*, *63*(7), 773–777, doi:10.5047/eps.2011.06.022.

Ide, S., and H. Aochi (2005), Earthquakes as multiscale dynamic ruptures with heterogeneous fracture surface energy, *J. Geophys. Res.*, *110*, B11303, doi:10.1029/2004JB003591.

Ide, S., A. Baltay, and G. C. Beroza (2011), Shallow Dynamic Overshoot and Energetic Deep Rupture in the 2011 Mw 9.0 Tohoku-Oki Earthquake, *Science*, *332*, 1426–1429, doi:10.1126/science.1207020.

Kato, A., K. Obara, T. Igarashi, H. Tsuruoka, S. Nakagawa, and N. Hirata (2012), Propagation of slow slip leading up to the 2011 *Mw* 9.0 Tohoku-Oki earthquake, *Science*, *335*(6069), 705–708, doi:10.1126/science.1215141.

Kendrick, E., M. Bevis, J. R. Smalley, B. Brooks, R. B. Vargas, E. Lauria, and L. P. Souto Fortes (2003), The Nazca-South America Euler vector and its rate of change, *J. South Am. Earth Sci.*, *16*(2), 125–131, doi:10.1016/S0895-9811(1003)00028-00022.

Kikuchi, M., and H. Kanamori (1991), Inversion of complex body waves-III, *Bull. Seismol. Soc. Am.*, *81*, 2335–2350.

Marsan, D., and B. Enescu (2012), Modeling the foreshock sequence prior to the 2011, M_W9.0 Tohoku, Japan, earthquake, *J. Geophys. Res.*, *117*, B06316, doi:10.1029/2011JB009039.

Moreno, M., et al. (2011), Heterogeneous plate locking in the South–Central Chile subduction zone: Building up the next great earthquake, *Earth Planet. Sci. Lett.*, *305*(3), 413–424, doi:10.1016/j.epsl.2011.03.025.

Noda, H., M. Nakatani, and T. Hori (2013), Large nucleation before large earthquakes is sometimes skipped due to cascade-up - Implications from a rate and state simulation of faults with hierarchical asperities, *J. Geophys. Res. Solid Earth*, *118*, 2924–2952, doi:10.1002/jgrb.50211.

Ohta, Y., et al. (2012), Geodetic constraints on afterslip characteristics following the March 9, 2011, Sanriku-oki earthquake, Japan, *Geophys. Res. Lett.*, *39*, L16304, doi:10.1029/2012GL052430.

Razafindrakoto, H. N., and P. M. Mai (2014), Uncertainty in Earthquake Source Imaging Due to Variations in Source Time Function and Earth Structure, *Bull. Seismol. Soc. Am.*, *104*(2), 855–874.

Stein, R. S. (1999), The role of stress transfer in earthquake occurrence, *Nature*, *402*(6762), 605–609.

Suito, H., T. Nishimura, M. Tobita, T. Imakiire, and S. Ozawa (2011), Interplate fault slip along the Japan Trench before the occurrence of the 2011 off the Pacific coast of Tohoku Earthquake as inferred from GPS data, *Earth Planets Space*, *63*(7), 615–619, doi:10.5047/eps.2011.06.053.

Wessel, P., and W. H. F. Smith (1998), New, improved version of generic mapping tools released, *Eos Trans. AGU*, *79*, 579.

Yabuki, T., and M. Matsu'ura (1992), Geodetic data inversion using a Bayesian information criterion for spatial distribution of fault slip, *Geophys. J. Int.*, *109*, 363–375.

Yagi, Y., and Y. Fukahata (2011a), Introduction of uncertainty of Green's function into waveform inversion for seismic source processes, *Geophys. J. Int.*, *186*, 711–720, doi:10.1111/j.1365-246X.2011.05043.x.

Yagi, Y., and Y. Fukahata (2011b), Rupture process of the 2011 Tohoku-oki earthquake and absolute elastic strain release, *Geophys. Res. Lett.*, *38*, L19307, doi:10.1029/2011GL048701.

Yagi, Y., M. Kikuchi, and T. Sagiya (2001), Co-seismic slip, post-seismic slip, and aftershocks associated with two large earthquakes in 1996 in Hyuga-nada, Japan, *Earth Planets Space*, *53*, 793–804, doi:10.5636/eps.53.793.